How to cite: *Angew. Chem. Int. Ed.* **2025**, e202504380
doi.org/10.1002/anie.202504380

CO_2 Reduction

Boosting Current Density of Electrocatalytic CO_2 Reduction using Metal–Enzyme Hybrid Cathodes

Yeomin Kang[+], Yunjae Kim[+], Youngjin Doh, Jinwoo Lee, Jungbae Kim,* and Ki Tae Park**

Abstract: As a promising solution to global warming, electrocatalytic reduction of carbon dioxide (CO_2RR) to liquid fuel has attracted great attention. A primary challenge in industrializing CO_2RR technologies for producing liquid fuel is the mass transfer limitation of CO_2, which significantly reduces the current density of CO_2RR. This study proposes a new enzyme-enhanced electrocatalysis platform for boosting CO_2RR current density. This platform integrates an enzyme of bovine carbonic anhydrase (bCA), stabilized on carbon nanotubes (bCA@CNT), into formate/formic acid selective metal catalysts such as tin (Sn) and bismuth (Bi) to prepare Metal-bCA (M-bCA) hybrid cathodes. The incorporation of bCA enhances both the CO_2 hydration and the reversible dehydration of bicarbonate to CO_2 in the cathode. This dynamic catalysis of bCA facilitates rapid local regeneration of dissolved CO_2 from bicarbonate at the catalyst surface, thereby boosting the current density of CO_2RR. Consequently, the formate current density of the Sn-bCA cathode was 3.3 times higher than that of the bare Sn cathode in a membrane-electrode assembly (MEA)-type cell. Furthermore, the Bi-bCA cathode achieved an excellent current density of 442 mA cm^{-2}, 1.5 times higher than the bare Bi cathode, for direct production of highly concentrated (3.4 mol L^{-1}) formic acid in a 3-compartment cell.

Carbon dioxide (CO_2), a major contributor to global warming and the climate crisis, has attracted considerable attention as a potential feedstock for the sustainable production of chemicals and fuels.[1–4] The CO_2RR for the synthesis of valuable products such as formate/formic acid, carbon monoxide, ethanol, and ethylene via the use of renewable electricity has been proposed as a promising strategy for closing the carbon cycle.[2–4] Over the past decade, considerable research efforts have been devoted to the development of highly selective electrocatalysts, appropriate electrolytes, and efficient reactor designs for industrial implementation of the CO_2RR technology.[3,5,6]

However, the CO_2RR still faces several challenges, including high overpotential arising from a high thermodynamic energy barrier, reduced Faradaic efficiency (FE) due to the competing hydrogen evolution reaction (HER), and limited reaction kinetics due to the flooding of electrodes.[3,7–9] In particular, electrode flooding is one of the most critical issues, which significantly reduces CO_2RR current density. This problem is particularly severe in membrane-electrode assembly (MEA)-type electrolyzers using cation exchange membranes (CEMs) for producing liquid products. In this system, the catalyst layer is continuously exposed to the produced liquid product, water, and cations from the anode during operation due to crossover. These harsh operational conditions of the cathode lead to flooding, which restricts CO_2 supply significantly and promotes HER, thereby limiting the current density of the CO_2RR process.[3,10,11] To overcome these challenges, ensuring a sufficient supply of CO_2 to the catalyst surface is essential to achieve high CO_2RR current density for liquid fuel production.

Natural metalloenzymes containing specific metal ions (e.g., Zn, Fe, and Ni) at the active site of the enzyme molecule have been studied for their application in bio-electrocatalytic CO_2 reduction reactions.[4,12–19] For example, carbonic anhydrase (CA) catalyzes the hydration of CO_2 to bicarbonate ion (HCO_3^-) at a turnover rate of approximately 10^6 molecules per second in vivo.[20] Due to this super-rapid CO_2 hydration ability, the CA enzyme has been studied as a CO_2 hydration promoter for bicarbonate-based CO_2-capture solvents and enzymatic CO_2 reduction catalysis.[12,21–25] Cobb et al. demonstrated that co-immobilizing CA with formate dehydrogenase (FDH) on an electrode significantly enhanced the kinetics of CO_2 hydration, which promoted the enzymatic reduction of CO_2 to formate.[12]

Tobolovskaya et al. demonstrated that the bicarbonate dehydration activity of bCA can be integrated with a CO_2RR electrolyzer to regenerate the CO_2 gas feed for the formation

[*] Y. Kang[+], Y. Doh, K. T. Park
Department of Chemical Engineering, Konkuk University, 120 Neungdong-ro, Gwangjin-gu, Seoul05029, Republic of Korea
E-mail: kpark@konkuk.ac.kr

Y. Kim[+], J. Kim
Department of Chemical and Biological Engineering, Korea University, 145 Anam-ro, Seongbuk-gu, Seoul02841, Republic of Korea
E-mail: jbkim3@korea.ac.kr

J. Lee
Department of Chemical and Biomolecular Engineering, Korea Advanced Institute of Science and Technology (KAIST), 291 Daehak-ro, Yuseong-gu, Daejeon34141, Republic of Korea
E-mail: jwlee1@kaist.ac.kr

[+] Both authors contributed equally to this work.

Additional supporting information can be found online in the Supporting Information section

of syngas. The bCA was immobilized on the back side of Au-coated carbon paper, which was then used as the cathode in a CO_2-saturated potassium bicarbonate ($KHCO_3$) solution.[21] The incorporation of bCA was effective in improving the current density of CO_2RR. They emphasized the dual functionality of bCA in catalyzing both the hydration of CO_2 to bicarbonate and the reverse dehydration process, supplying CO_2 as a feed for CO_2RR. However, in their system, the bCA was positioned separately from the catalytic interface, either behind the electrode or in the electrolyte, leading to limited catalytic benefits due to diffusion constraints. Moreover, the poor stability of bCA has highlighted the need for improved enzyme–electrocatalyst integration designs and strategies for the enhancement of bCA stability.

In the majority of studies in this field, a lack of knowledge regarding enzyme immobilization and stabilization has led to CA being simply adsorbed on nanomaterials or being used as a free enzyme, thereby ending up with poor activity and stability of enzymes.[12,21–24] However, enzymes can be effectively immobilized by using nanomaterials to produce highly loaded and stabilized nano-biocatalysts via chemical cross-linking of enzyme molecules.[26–30] In particular, using an approach via three steps of "Enzyme Adsorption, Precipitation, and Crosslinking (EAPC)," both superior enzyme loading/activity and even long-term enzyme stability could be achieved when compared to those prepared using simple adsorption and covalent attachment methods.[26,27]

Here, we propose a novel bio-enhanced electrocatalytic platform of metal-enzyme (M-bCA) hybrid cathodes to enhance the current density of CO_2RR for formate/formic acid production. To achieve high and stable bCA activity, bCA was immobilized on carbon nanotubes (CNT) via the EAPC method. The resulting bCA@CNT with highly-stabilized and highly-loaded bCA was then integrated into formate/formic acid-selective metal catalysts, such as tin (Sn) and bismuth (Bi),[31–34] to fabricate M-bCA hybrid cathodes. These hybrid electrodes utilize the ability of bCA to accelerate both the CO_2 hydration to bicarbonate and the reversible dehydration of bicarbonate back to CO_2.[35] Therefore, even under flooding conditions, where the formation of an aqueous layer on the catalyst surface hinders CO_2 transport, the rapid and reversible catalysis of bCA within the cathode layer can facilitate efficient local CO_2 supply to the catalyst surface, as illustrated in Scheme 1. To evaluate the resulting enhancement in current density, the CO_2RR performance of the M-bCA hybrid cathodes was systematically investigated using H-type, MEA-type, and three-compartment cell configurations.

The bCA@CNT with high bCA loading and stability was successfully prepared via the EAPC approach, as schematically shown in Figure 1a. The scanning electron microscopy (SEM) images of bare CNT and bCA@CNT, prepared via an EAPC method, are shown in Figure 1b,c, respectively, wherein the dramatically increased thickness of EAPC (Figure 1c) compared with the bare CNT (Figure 1b) is evidently shown. This result indicates that the EAPC approach achieves a high enzyme loading via an effective combination of enzyme precipitation and crosslinking. Based on elemental analysis and quantification of the nitrogen (N) atoms, originating only from the enzyme molecules, the enzyme loading was estimated to be 7.4 unit-bCA/mg-CNT. One unit-bCA is defined as the amount of bCA required to hydrolyze 1 μmol of 4-nitrophenyl acetate (NPA) per minute in 100 mM sodium phosphate buffer (pH 7.6). Ideally, when 1 unit-bCA is loaded per 1 cm^2 of electrode area, the rapid enzymatic kinetics corresponds to a rate of 1.7×10^{-5} mol s^{-1} cm^{-2} for CO_2 hydration or bicarbonate dehydration. If CO_2 is supplied to the catalyst at this rate, the theoretical CO_2RR current density could reach approximately 3.2 A cm^{-2}.

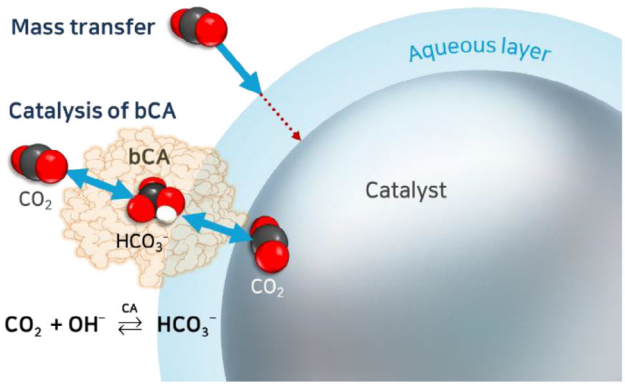

Scheme 1. Schematic diagram of the metal-enzyme hybrid electrocatalytic platform illustrating sufficient CO_2 supply facilitated by fast and reversible catalysis of bCA.

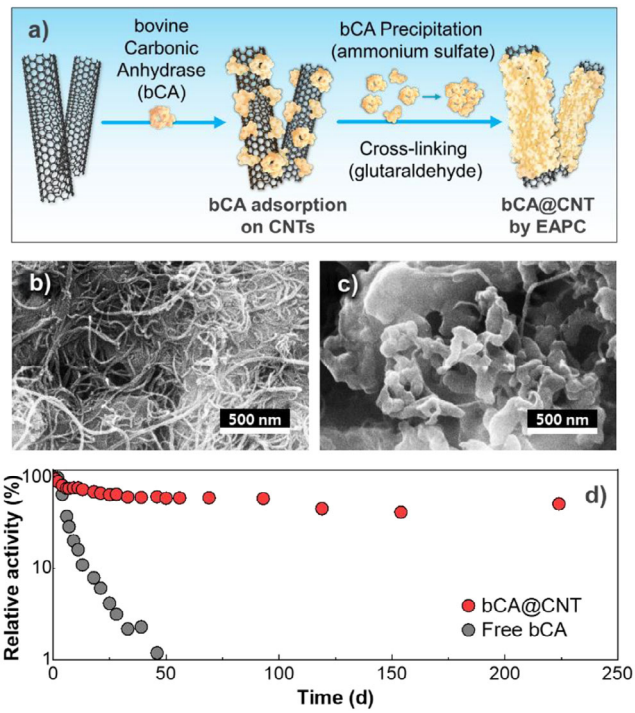

Figure 1. a) Schematic preparation of bCA@CNT via the approach of enzyme adsorption, precipitation, and crosslinking (EAPC) approach. b,c) SEM images of (b) CNT and (c) bCA@CNT. d) Enzyme stabilities of free bCA and bCA@CNT.

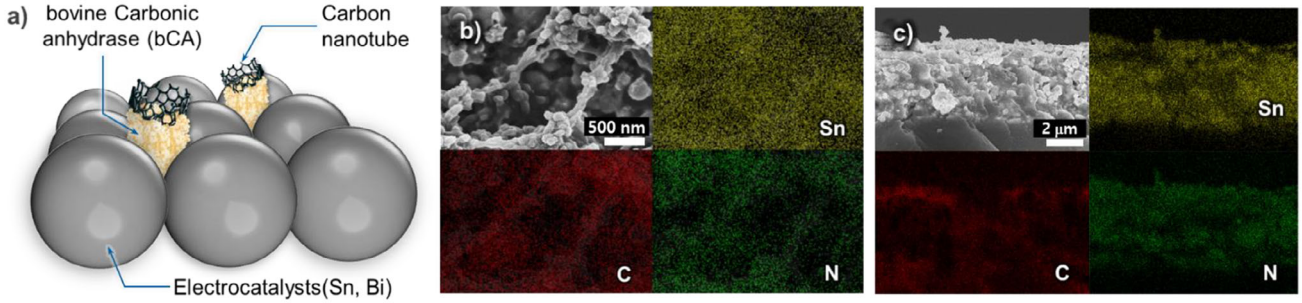

Figure 2. a) Schematic illustration of the M-bCA hybrid cathodes. FE-SEM and EDS mapping images (Sn, C, and N) of the Sn-bCA hybrid electrode for MEA-type cell measurements: b) top of surface view, and c) cross-sectional view.

The bCA stability of bCA@CNT, compared to free bCA, is shown in Figure 1d. The free bCA showed a monotonous decrease in its enzyme activity, and its half-life was estimated to be 3.52 d. On the other hand, the bCA@CNT exhibited a biphasic inactivation curve with significantly greater enzyme stability than free bCA. After the initial activity drop due to the inactivation of poorly immobilized enzyme molecules during the first 9 days, its half-life was estimated to be 347 d (Figure 1d). Notably, the half-life of bCA@CNT was 99 times longer than that of free bCA (3.52 d).

Figure 2a presents a schematic illustration of the M-bCA hybrid cathodes, where bCA@CNTs are physically mixed within the metal (Sn or Bi) catalyst layers. Sn-bCA cathodes with a bCA loading of 15×10^3 unit cm^{-2} were prepared by the spray coating method onto carbon paper (TGPH-060, Toray) for H-type cell measurements (Figure S1) and on a Nafion 115 membrane for MEA-type cell measurements (Figure S2). The loading amounts of Sn, bCA, and CNT of the prepared cathodes are given in Tables S1 and S2. The carbon (C) and nitrogen (N) energy dispersive X-ray spectroscopy (EDS) mapping images of the Sn-bCA cathodes are shown in Figure 2b,c and Figure S2, wherein the uniform dispersion of the bCA@CNTs in the catalyst layer can be observed.

Figure 3 presents the results of the H-type cell measurements (Figure S4) of the Sn-bCA, Sn-CNT, and Sn cathodes. To investigate the effect of CNTs in the Sn cathode, an Sn-CNT cathode was prepared with the same CNT loading of 2.0 μg cm^{-2} as the Sn-bCA cathode. Figure 3a–d shows that Sn-bCA cathode exhibited electrochemical characteristics comparable to those of the bare Sn cathode, including a similar CV curve (Figure 3a), slightly lower charge transfer resistance (R_{CT}) (Figure 3b) and Tafel slope (Figure 3c), and a slightly higher electrochemical surface area (ECSA)(Figure 3d). However, the two electrodes exhibited a significant difference in CO_2RR performance. The bare Sn cathode exhibited a maximum FE_{HCOO^-} of 77.2% at −1.1 V (vs. RHE). However, as the reduction potential became more negative, the FE_{HCOO^-} decreased significantly, dropping to 30.4% at −1.7 V (vs. RHE) (Figure 3e). This substantial decrease in the formate selectivity can be contributed to the limited CO_2 supply.[36] This limitation is further supported by the observation that the j_{HCOO^-} for the Sn cathode did not increase with applied potentials below −1.1 V (vs. RHE), as shown in Figure 3f. The plateau in j_{HCOO^-} for bare Sn cathode highlights the challenges of achieving high current densities under CO_2 mass transport-limited conditions.

On the other hand, the Sn-bCA cathode demonstrated superior CO_2RR performance compared to the bare Sn cathode. As shown in Figure 3e, the Sn-bCA cathode achieved higher FE_{HCOO^-} than the bare Sn cathode at a reduction potential below −1.3 V (vs. RHE). Moreover, j_{HCOO^-} increased with the applied reduction potential, and reached approximately twice the value of the bare Sn cathode at −1.7 V (vs. RHE), as shown in Figure 3f. This trend reflects the growing importance of bCA under high current density conditions, where CO_2 is rapidly depleted near the catalyst surface. In such regimes, bCA promotes local CO_2 regeneration from bicarbonate, sustaining formate production beyond the diffusion limit. Control experiments with a bCA@CNT electrode without metal catalysts such as Sn and Bi confirmed that bCA itself is not electrochemically active and does not participate in charge-transfer reactions (Figure S5). In addition, as shown in Figure S6, increasing the $KHCO_3$ concentration led to higher FE_{HCOO^-} and j_{HCOO^-} values, suggesting that sufficient bicarbonate availability enhances bCA-mediated CO_2 supply, thereby improving both the selectivity and rate of CO_2RR.

It is crucial to understand how the bCA in the Sn cathode enables enhanced CO_2RR current density beyond the CO_2 mass transfer limits. To verify the proposed mechanism of rapid bicarbonate-to-CO_2 regeneration catalyzed by bCA, a set of comparative CO_2 absorption ($CO_2 + OH^- \rightarrow HCO_3^-$) and desorption ($HCO_3^- \rightarrow CO_2 + OH^-$) experiments were conducted in 0.5 M $KHCO_3$, both with and without bCA, as shown in Figure S7. The observed pH changes confirmed that bCA catalyzes and accelerates both the hydration of CO_2 and the reversible dehydration of bicarbonate.

To further investigate the bicarbonate-to-CO_2 regeneration mechanism, CO_2RR experiments were carried out in an H-type cell with bare metal (Sn and Bi) and M-bCA hybrid cathodes, using 1.0 M $KHCO_3$ solutions under an Ar atmosphere instead of CO_2. As shown in Figure S8, under an Ar atmosphere without external CO_2 supply, the bare Sn and Bi cathodes exhibited negligible CO_2RR activity, with FE_{HCOO^-} of approximately 1% and j_{HCOO^-} below 1 mA cm^{-2}. In contrast, the Sn-bCA and Bi-bCA hybrid cathodes demonstrated significantly enhanced CO_2RR activity, achieving maximum FE_{HCOO^-} values of 37.2% and

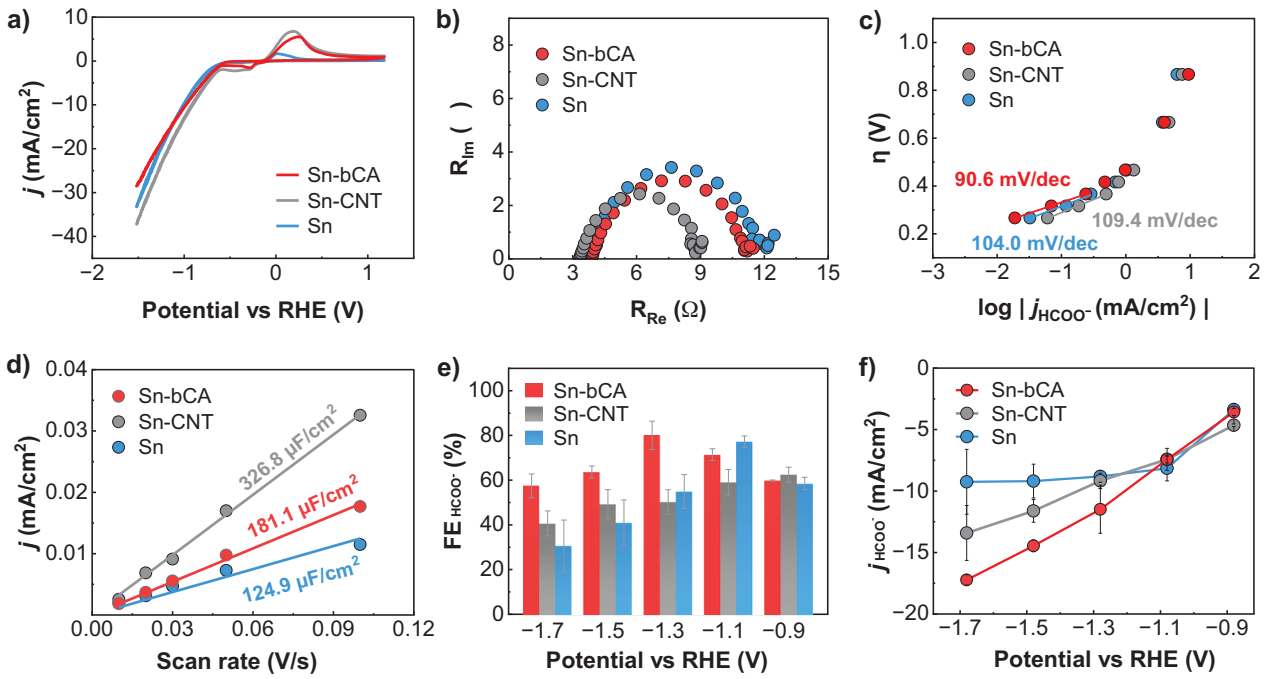

Figure 3. Results of H-type cell measurements of Sn-bCA, Sn-CNT, and Sn cathodes. a) CV curves (−1.5 to 1.2 V vs. RHE, 30 mV s^{-1} scan rate, CO_2-saturated 0.5 M $KHCO_3$), b) Nyquist impedance plots (1 MHz to 500 mHz, −0.8 V vs. RHE, 10 mV amplitude, CO_2-saturated 0.5 M $KHCO_3$), c) Tafel plots, d) electrochemical surface areas (ECSA) (see also Figure S3), e) formate Faradaic efficiency (FE_{HCOO^-}), and f) formate current density (j_{HCOO^-}).

44.6%, respectively, and j_{HCOO^-} values nearly 10 times higher than those of the bare metal electrodes.

In the absence of externally supplied CO_2, the concentration of dissolved CO_2 in the electrolyte is governed by the equilibrium between bicarbonate and CO_2. However, the equilibrium CO_2 concentration in a 1.0 M $KHCO_3$ solution at 25 °C is extremely low (approximately 0.01 M), making it difficult for CO_2RR to proceed efficiently on the bare Sn and Bi cathodes. In addition, when CO_2 is consumed at the catalyst surface by CO_2RR, it must be replenished through the equilibrium-driven dehydration of bicarbonate. However, the intrinsic rate constant for bicarbonate dehydration is relatively low ($k \approx 0.037$ s^{-1} at 25 °C).[20] In contrast, in the presence of bCA, the reaction rate is dramatically accelerated, with a catalytic rate constant (k_{cat}) reported to be on the order of 10^6 s^{-1}.[20] This rapid catalysis of bCA facilitates local regeneration of CO_2 from bicarbonate at the catalyst surface, enabling CO_2RR on M-bCA hybrid electrodes even under an Ar atmosphere. These results suggest that although bicarbonate cannot directly participate as a reactant in CO_2RR, it acts as a CO_2 reservoir that can be rapidly converted into CO_2 through bCA catalysis.[37–39]

As shown in Figure 3a,b,d, introducing a small amount of CNTs into the Sn catalyst layer increased the reduction current in the CV curves, reduced the R_{CT}, and increased the electrochemical surface area (ECSA). These results can be attributed to the ability of CNT to provide additional pathways for electron transport and facilitate better reactant distribution in the catalyst layer.[40–42] These properties of CNT led to an improvement in j_{HCOO^-} for the Sn-CNT cathode compared to the Sn cathode at reduction potentials below −1.3 V (vs. RHE) as shown in Figure 3f. However, Sn-CNT cathode achieved a maximum FE_{HCOO^-} of only 62.4% at −0.9 V (vs. RHE), which was the lowest formate selectivity among the tested electrodes (Figure 3e). This observation indicates that although introducing CNT into the catalyst layer enhanced the current density of CO_2RR, it decreased formate selectivity by more favorably promoting HER.

However, compared to the Sn-CNT cathode, the Sn-bCA hybrid cathode exhibited a lower reduction current in CV (Figure 3a), higher R_{CT} (Figure 3b), and a smaller ECSA (Figure 3d). This indicates that the beneficial effects of CNT were largely mitigated when bCA was immobilized on CNT due to the non-conductive nature of bCA molecules. In addition, the higher FE_{HCOO^-} observed for Sn-bCA relative to Sn-CNT (Figure 3e) suggests that the bCA molecules covering the CNT walls effectively suppress the HER on CNT. Furthermore, to investigate the importance of CNT-based immobilization, a Sn/free-bCA cathode, prepared by directly applying free-bCA onto the Sn catalyst layer without immobilization on CNT was evaluated. The Sn/free-bCA cathode exhibited significantly lower CO_2RR performance for formate production compared to the Sn-bCA cathode, with performance levels similar to those of the bare Sn cathode, as shown in Figure S5. This low performance is attributed to the poor stability of free bCA under electrolysis conditions, where it was easily detached from the electrode surface due to electrolyte flow and hydrogen evolution. These results demonstrate that CNT in the bCA@CNT architecture plays a crucial role in immobilizing and stabilizing bCA

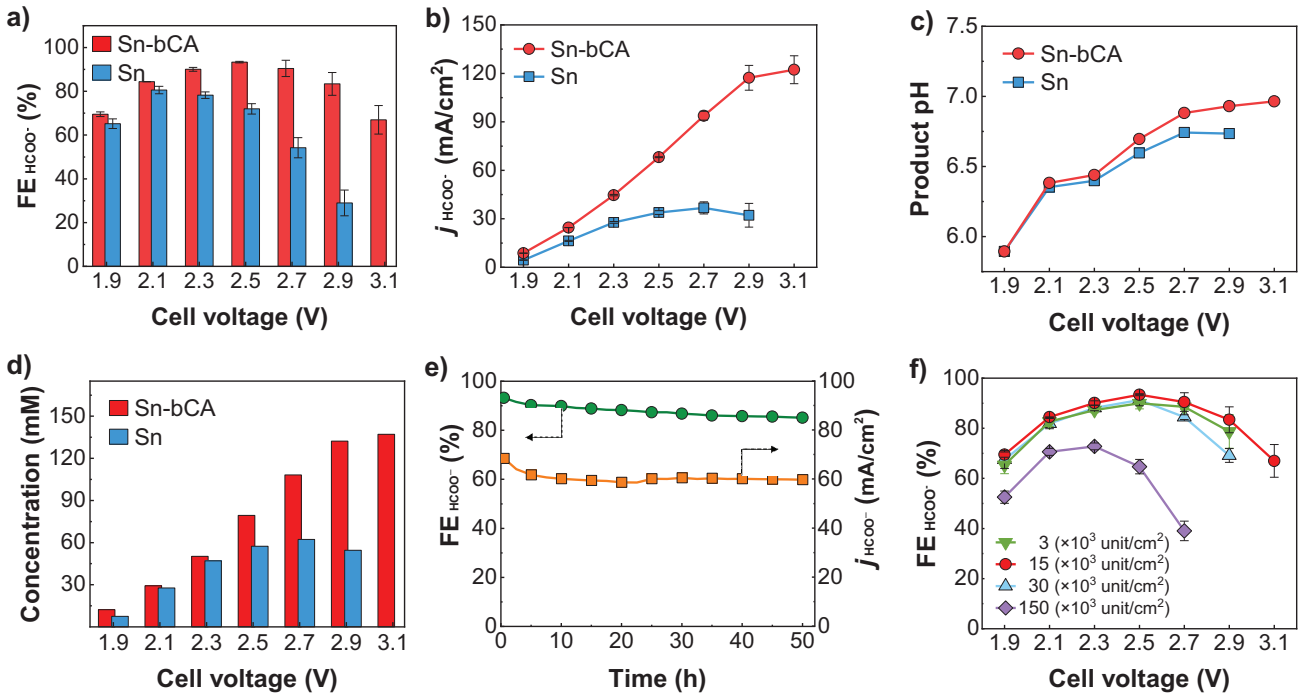

Figure 4. Comparison of CO_2RR performances in MEA-type cells between Sn-bCA and Sn cathodes. a) Formate Faradaic efficiency (FE_{HCOO^-}), b) formate current density (j_{HCOO^-}), c) pH value of the liquid product, and d) formate concentration in the liquid product at different cell voltages. e) CO_2RR performance of the Sn-bCA hybrid cathode over 50 h of operation at a cell voltage of 2.5 V. f) Dependence of FE_{HCOO^-} on bCA loadings in Sn-bCA hybrid cathode.

molecules. Meanwhile, the enhanced FE_{HCOO^-} and twofold increase in j_{HCOO^-} observed with the Sn-bCA hybrid cathode are primarily attributed to the contribution of bCA in bCA@CNT.

The superior CO_2RR performance of the Sn-bCA hybrid cathode was more clearly demonstrated in the MEA-type cell configuration (Figure S9). Figure 4a,b presents the FE_{HCOO^-} and j_{HCOO^-} of the Sn-bCA and bare Sn cathodes in the MEA-type cell as a function of the applied cell voltage. Figure S10 shows that the sum of FE_{HCOO^-} and FE_{H2} reached approximately 99%, and the FE_{CO} was around 1%. For the bare Sn cathode, the FE_{HCOO^-} reached a maximum value of 80.6% at 2.1 V but decreased sharply to 28.9% at 2.9 V (Figure 4a). In addition, the j_{HCOO^-} of Sn cathode was limited to 36.7 mA cm^{-2} at 2.7 V. This poor CO_2RR performance of the Sn cathode clearly illustrated the flooding issue commonly observed in MEA-type cells employing CEMs for liquid product recovery. In this configuration, the catalyst layer is continuously exposed to water and K^+ ions migrate from the anode. Furthermore, the liquid product (formate solution) is discharged in the direction opposite to the CO_2 gas supply. These harsh conditions significantly limit the CO_2 supply and the current density of CO_2RR.[10]

In contrast, the Sn-bCA hybrid cathode maintained high FE_{HCOO^-} even above 2.1 V, reaching a maximum FE_{HCOO^-} of 93.4% at 2.5 V (Figure 4a). Notably, it exhibited a remarkable improvement in j_{HCOO^-}, as shown in Figure 4b. The Sn-bCA hybrid cathode showed a continuous increase in j_{HCOO^-} with increasing cell voltage, achieving 122.3 mA cm^{-2}, whereas the bare Sn cathode showed a limited j_{HCOO^-} of 36.7 mA cm^{-2} above 2.7 V. The j_{HCOO^-} achieved by the Sn-bCA hybrid cathode was 3.3 times higher than that of the bare Sn cathode. These results provide experimental evidence that the Sn-bCA hybrid cathode exceeds the CO_2 diffusion-limited current density observed for the bare Sn electrode, confirming that bCA-mediated local CO_2 regeneration effectively alleviates mass transport limitations under high current density operation. These findings clearly demonstrate the beneficial role of bCA incorporation into the Sn cathode, ensuring a sustained local CO_2 supply and enabling continuous increases in j_{HCOO^-} with increasing cell voltage. As a result, the Sn-bCA hybrid cathode effectively overcomes the CO_2RR current density limitations caused by flooding in MEA-type cells.

As shown in Figure 4c, the pH of the liquid product recovered by the Sn-bCA hybrid cathode in the MEA-type cell was investigated. As the cell voltage increased from 1.9 to 3.1 V, the pH rose from 5.9 to 7.0, primarily because the formate concentration in the product increased with increasing j_{HCOO^-}, as shown in Figure 4d. The increased formate concentration, driven by the boosted j_{HCOO^-} at the Sn-bCA cathode, led to a higher pH in the liquid product compared to that at the Sn cathode (Figure 4c). This increased pH environment at the Sn-bCA hybrid cathode was favorable for CO_2RR and effectively suppressed the HER (Figure S11).

Figure 4e shows stable CO_2RR performance of the Sn-bCA hybrid electrode over 50 h of continuous operation at 2.5 V. The stability test shows that both the FE_{HCOO^-} and j_{HCOO^-} remained consistent during the period of 50 h, indicating that the Sn-bCA cathode retained stable catalytic activity without significant degradation. As shown in Figure S12, the

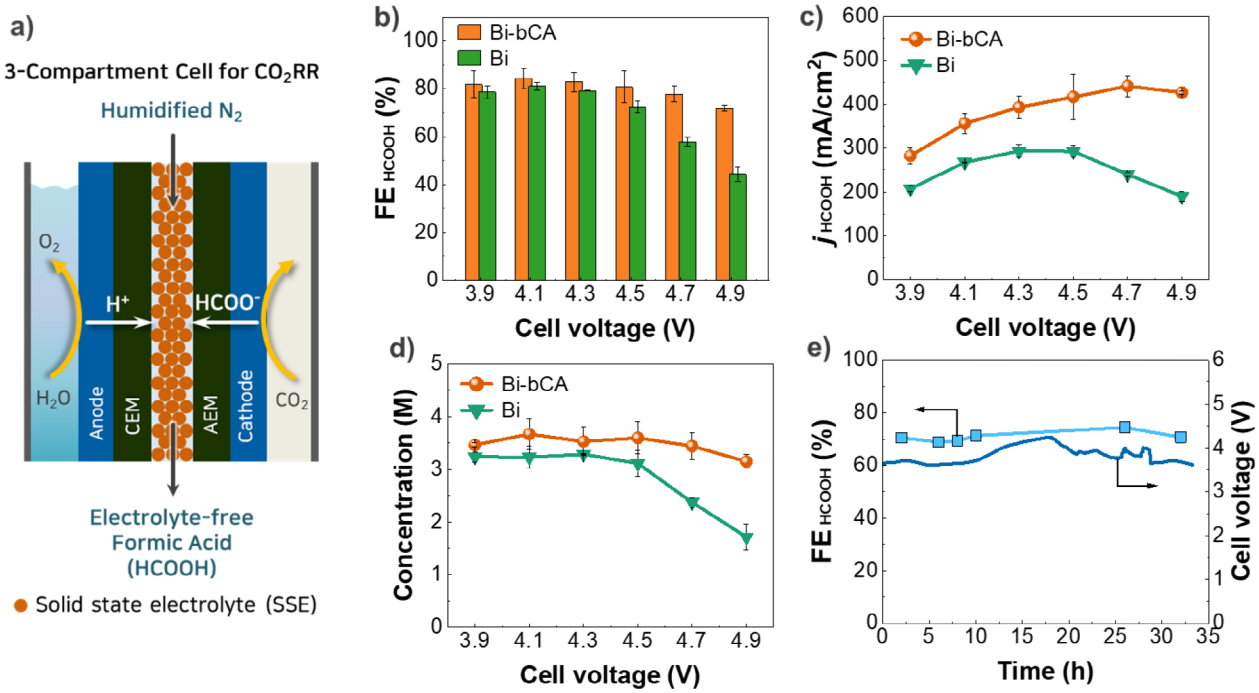

Figure 5. a) Configuration of the 3-compartment cell for CO_2RR. Comparison of CO_2RR performances in the 3-compartment cell between Bi-bCA and Bi cathodes. b) Formic acid Faradaic efficiency (FE_{HCOOH}), c) formic acid current density (j_{HCOOH}), and d) formic acid concentration in the liquid product at different cell voltages. e) CO_2RR performance of the Bi-bCA hybrid cathode over 32 h of operation at a current density of 300 mA cm^{-2}.

SEM images, X-ray diffraction (XRD) patterns, and the Sn 3d X-ray photoelectron spectroscopy (XPS) spectra before and after the 50 h operation indicate that the overall morphology, crystalline structure, and surface chemical state of the Sn-bCA cathode remained largely stable. Minor morphological changes, such as mild surface roughening and the formation of nanoscale bumps, were observed, but these did not affect the crystal structure or catalytic activity. In addition, enzyme activity measurements after 50 h of electrolysis, summarized in Table S4, confirmed that the bCA retained 95.29% of its initial activity, indicating excellent long-term stability of the bCA@CNT under operating conditions.

Additionally, it is important to determine the appropriate bCA loading amount because the bCA itself is not a catalyst for CO_2RR. Figure 4f and Figure S13 show how the CO_2RR performance varies with bCA loading in the range of 3–150 ($\times 10^3$ unit cm^{-2})(Table S5). The Sn-bCA cathode with bCA loading of 15 ($\times 10^3$ unit cm^{-2}) achieved the highest FE_{HCOO^-} and j_{HCOO^-}, whereas a loading of 150 ($\times 10^3$ unit cm^{-2} resulted in poorer performance than the bare Sn cathode. This result suggests that excessive loading of non-conductive bCA can reduce the overall electrocatalytic activity of the Sn-bCA hybrid cathode.

In addition, a Bi-bCA hybrid cathode was prepared (Figure S14) and tested in a 3-compartment cell for formic acid (HCOOH) production to demonste the current density enhancement of M-bCA hybrid cathodes. Recently, several research groups have reported 3-compartment cell designs that employ a solid-state electrolyte (SSE) compartment between the anode and cathode, enabling direct production of electrolyte-free formic acid instead of formate mixed with electrolytes.[32,43–46] As shown in Figure 5a, the cathode and anode each contact an anion exchange membrane (AEM) and a cation exchange membrane (CEM), respectively. The $HCOO^-$ and H^+ ions generated at the cathode and anode migrate across the AEM and CEM, respectively, into the central SSE compartment, where they combine to form electrolyte-free HCOOH. In this system, cathode flooding is significantly mitigated compared to MEA-type cells using CEMs, because the liquid product is recovered from the center compartment without electrolyte solutions.

Figure 5b,c shows the superior CO_2RR performance of the Bi-bCA hybrid cathode compared to the bare Bi cathode for HCOOH production. In particular, Bi-bCA exhibited higher j_{HCOOH}, which increased with increasing cell voltage up to 4.7 V, whereas the Bi cathode showed limited j_{HCOOH} above 4.3 V. The Bi-bCA hybrid cathode achieved a maximum j_{HCOOH} of 442 mA cm^{-2} at 4.7 V, which is 1.5 times higher than that of the bare Bi cathode (293 mA cm^{-2} at 4.3 V). As a result, an electrolyte-free HCOOH solutions with high concentrations of 3.1–3.7 mol L^{-1} (M) were produced by the Bi-bCA hybrid cathode (Figure 5d). In addition, the Bi-bCA cathode was stably operated at a current density of 300 mA cm^{-2} for 32 h (Figure 5e). This reveals that bCA effectively functions in the Bi cathode within the 3-compartment cell system. Overall, these findings have demonstrated that the introduction of M-bCA hybrid cathode into an appropriate electrolyzer can significantly enhance the current density of CO_2RR to liquid fuels (Table S6).

In summary, we developed an enzyme-enhanced electrocatalysis platform based on metal-enzyme (M-bCA) hybrid cathodes that overcomes conventional CO_2 mass transfer

limitations in CO_2RR. Through an enzyme adsorption, precipitation, and crosslinking (EAPC) method, bCA was stably immobilized on CNTs and integrated into Sn and Bi catalyst layers. The Sn-bCA cathode exhibited a 3.3-fold increase in j_{HCOO^-} compared to bare Sn in an MEA-type cell, while the Bi-bCA cathode delivered a j_{HCOO^-} of 442 mA cm^{-2}, 1.5 times higher than that of bare Bi, in a three-compartment system. These enhancements are attributed to the dynamic catalysis of bCA, which enables rapid and sustained local CO_2 regeneration from bicarbonate at the catalyst surface. The enhanced CO_2RR current densities achieved with the M-bCA platform in MEA-type and three-compartment cells highlight its strong potential for scalable, energy-efficient, and selective CO_2 conversion, with versatility across various CO_2RR products beyond formate and formic acid. Further improvements may be achieved by co-immobilizing bCA and metal catalysts on a single support, such as CNTs, to enhance local catalytic synergy. Additionally, detailed mechanistic modeling to optimize local CO_2 concentration and product mass transport could contribute significantly to achieving quantitative yields on metal-enzyme hybrid electrodes.

Acknowledgements

This work was supported by the National Research Foundation of Korea (NRF) grant funded by the Korea government (MSIT) (No.2020R1A2C3009649 and No.2022M3C1A3081432) and Human Resources Development Program of the Korea Institute of Energy Technology Evaluation and Planning (KETEP) grant funded by the Ministry of Trade, Industry and Energy, Republic of Korea (No. RS-2023–00237035).

Conflict of Interests

The authors declare no conflict of interest.

Data Availability Statement

The data that support the findings of this study are available from the corresponding author upon reasonable request.

Keywords: Carbonic anhydrase • CO_2 reduction • Electrocatalysis • Enzyme • Flooding

[1] Y. Y. Birdja, E. Pérez-Gallent, M. C. Figueiredo, A. J. Göttle, F. Calle-Vallejo, M. T. M. Koper, *Nat. Energy* **2019**, *4*, 732–745.
[2] J. Lee, W. Lee, K. H. Ryu, J. Park, H. Lee, J. H. Lee, K. T. Park, *Green Chem.* **2021**, *23*, 2397–2410.
[3] W. Lee, Y. E. Kim, M. H. Youn, S. K. Jeong, K. T. Park, *Angew. Chem. Int. Ed.* **2018**, *57*, 6883–6887.
[4] X. Tan, J. Nielsen, *Chem. Soc. Rev.* **2022**, *51*, 4763–4785.
[5] Y. Xie, P. Ou, X. Wang, Z. Xu, Y. C. Li, Z. Wang, J. E. Huang, J. Wicks, C. McCallum, N. Wang, Y. Wang, T. Chen, B. T. W. Lo, D. Sinton, J. C. Yu, Y. Wang, E. H. Sargent, *Nat. Catal.* **2022**, *5*, 564–570.
[6] S. D. Rihm, M. K. Kovalev, A. A. Lapkin, J. W. Ager, M. Kraft, *Energy Environ. Sci.* **2023**, *16*, 1697–1710.
[7] M. Li, M. N. Idros, Y. Wu, T. Burdyny, S. Garg, X. S. Zhao, G. Wang, T. E. Rufford, *J. Mater. Chem. A* **2021**, *9*, 19369–19409.
[8] E. R. Cofell, U. O. Nwabara, S. S. Bhargava, D. E. Henckel, P. J. A. Kenis, *ACS Appl. Mater. Interfaces* **2021**, *13*, 15132–15142.
[9] P. Kamat, P. Christopher, *ACS Energy Lett.* **2022**, *7*, 1469–1472.
[10] H. Rabiee, L. Ge, X. Zhang, S. Hu, M. Li, Z. Yuan, *Energy Environ. Sci.* **2021**, *14*, 1959–2008.
[11] B. Chang, H. Pang, F. Raziq, S. Wang, K.-W. Huang, J. Ye, H. Zhang, *Energy Environ. Sci.* **2023**, *16*, 4714–4758.
[12] S. J. Cobb, V. M. Badiani, A. M. Dharani, A. Wagner, S. Zacarias, A. R. Oliveira, I. A. C. Pereira, E. Reisner, *Nat. Chem.* **2022**, *14*, 417–424.
[13] L. Luan, X. Ji, B. Guo, J. Cai, W. Dong, Y. Huang, S. Zhang, *Biotechnol. Adv.* **2023**, *63*, 108098.
[14] Y. Guo, X. Hong, Z. Chen, Y. Lv, *J. Energy Chem.* **2023**, *80*, 140–162.
[15] S. J. Cobb, S. Rodriguez-Jimenez, E. Reisner, *Angew. Chem. Int. Ed.* **2023**, *63*, e202310547.
[16] H. Chen, Y. Huang, C. Sha, J. M. Moradian, Y.-C. Yong, Z. Fang, *Renew. Sustain. Energy Rev.* **2023**, *178*, 113271.
[17] M. Mao, T. Zhai, L. Meng, Z. Meng, W. Liu, *Chem. Eng. J.* **2022**, *437*, 135479.
[18] H. Song, C. Ma, P. Liu, C. You, J. Lin, Z. Zhu, *J. CO2 Util.* **2019**, *34*, 568–575.
[19] B. S. Jayathilake, S. Bhattacharya, N. Vaidehi, S. R. Narayanan, *Acc. Chem. Res.* **2019**, *52*, 676–685.
[20] R. G. Khalifah, *J. Biol. Chem.* **1971**, *246*, 2561–2573.
[21] Y. Tobolovskaya, J. J. Medvedev, X. V. Medvedeva, M. S. Mesbahuddin, N. E. N. Rodriguez, S. Kalyaanamoorthy, A. Klinkova, *J. CO2 Util.* **2023**, *71*, 102461.
[22] Y. Zhang, J. Zhu, J. Hou, S. Yi, B. Van der Bruggen, Y. Zhang, *J. Membrane Sci. Lett.* **2022**, *2*, 100031.
[23] J. K. J. Yong, G. W. Stevens, F. Caruso, S. E. Kentish, *J. Chem. Technol. Biotechnol.* **2015**, *90*, 3–10.
[24] A. G. Fink, E. W. Lees, J. Gingras, E. Madore, S. Fradette, S. A. Jaffer, M. Goldman, D. J. Dvorak, C. P. Berlinguette, *J. Inorg. Biochem.* **2022**, *231*, 111782.
[25] H. S. Kim, S.-G. Hong, J. Yang, Y. Ju, J. Ok, S.-J. Kwon, K.-M. Yeon, J. S. Dordick, J. Kim, *J. CO2 Util.* **2020**, *38*, 291–298.
[26] T. S. Kim, J. Nam, D. W. Kim, H. T. Jung, K. M. Yeon, J. Kim, *Chem. Eng. J.* **2021**, *424*, 130343.
[27] T. H. Kim, I. Lee, K. M. Yeon, J. Kim, *J. Membr. Sci.* **2018**, *554*, 357–365.
[28] S. G. Hong, H. Jeon, H. S. Kim, S. H. Jun, E. Jin, J. Kim, *Environ. Sci. Technol.* **2015**, *49*, 4466–4472.
[29] H. S. Kim, S. G. Hong, K. M. Woo, V. T. Seijas, S. Kim, J. Lee, J. Kim, *ACS Catal.* **2018**, *8*, 6526–6536.
[30] S. H. Jun, J. Yang, H. Jeon, H. S. Kim, S. P. Pack, E. Jin, J. Kim, *Environ. Sci. Technol.* **2020**, *54*, 1223–1231.
[31] D. Tan, W. Lee, K. T. Park, Y. E. Jeon, J. Hong, Y. N. Ko, Y. E. Kim, *Appl. Surf. Sci.* **2023**, *613*, 155944.
[32] R. Nankya, Y. Xu, A. Elgazzar, P. Zhu, T. U. Wi, C. Qiu, Y. Feng, F. Che, H. Wang, *Angew. Chem. Int. Ed.* **2024**, *63*, e202403671.
[33] X. Wang, Y. Zhang, S. Wang, Y. Li, Y. Feng, Z. Dai, Y. Chen, X. Meng, J. Xia, G. Zhang, *Angew. Chem* **2024**, *136*, e202407665.
[34] W. Guo, X. Cao, D. Tan, B. Wulan, J. Ma, J. Zhang, *Angew. Chem. Int. Ed.* **2024**, *63*, e202401333.
[35] H. DeVoe, G. B. Kistiakowsky, *J. Am. Chem. Soc.* **1961**, *83*, 274–280.
[36] E. W. Lees, B. A. W. Mowbray, F. G. L. Parlane, C. P. Berlinguette, *Nat. Rev. Mater.* **2021**, *7*, 55–64.
[37] H. Huang, W. Zhang, M. Li, Y. Gan, J. Chen, Y. Kuang, *J. Colloid Interface Sci.* **2005**, *284*, 593–599.
[38] J. Zeng, M. Fontana, A. Sacco, D. Sassone, C. F. Pirri, *Catal. Today*, **2022**, *397–399*, 463–474.

[39] X. Wang, Q. Chen, Y. Zhou, Y. Tan, Y. Wang, H. Li, Y. Chen, M. Sayed, R. A. Geioushy, N. K. Allam, J. Fu, Y. Sun, M. Liu, *Nano Res.* **2024**, *17*, 1101–1106.
[40] A. Wuttig, Y. Yoon, J. Ryu, Y. Surendranath, *J. Am. Chem. Soc.* **2017**, *139*, 17109–17113.
[41] S. Zhu, B. Jiang, W.-B. Cai, M. Shao, *J. Am. Chem. Soc.* **2017**, *139*, 15664–15667.
[42] T. Li, E. W. Lees, M. Goldman, D. A. Salvatore, D. M. Weekes, C. P. Berlinguette, *Joule* **2019**, *3*, 1487–1497.
[43] H. Yang, J. J. Kaczur, S. D. Sajjad, R. I. Masel, *J. CO2 Util* **2017**, *20*, 208–217.
[44] L. Fan, C. Xia, P. Zhu, Y. Lu, H. Wang, *Nat. Commun.* **2020**, *11*, 3633.
[45] C. Xia, P. Zhu, Q. Jiang, Y. Pan, W. Liang, E. Stavitski, H. N. Alshareef, H. Wang, *Nat. Energy* **2019**, *4*, 776–785.
[46] H. Yang, J. J. Kaczur, S. D. Sajjad, R. I. Masel, *J. CO2 Utili* **2020**, *42*, 101349.

Manuscript received: February 22, 2025
Revised manuscript received: April 15, 2025
Accepted manuscript online: April 25, 2025
Version of record online: ■■, ■■

Communication

CO_2 Reduction

Y. Kang, Y. Kim, Y. Doh, J. Lee*, J. Kim*, K. T. Park* **e202504380**

Boosting Current Density of Electrocatalytic CO_2 Reduction using Metal–Enzyme Hybrid Cathodes

A metal-enzyme (M-bCA) hybrid platform integrates highly stabilized and densely loaded bovine carbonic anhydrase (bCA) immobilized on CNTs with Sn and Bi catalysts. The enzyme dynamically catalyzes the reversible interconversion between CO_2 and bicarbonate, enabling rapid local CO_2 regeneration at the catalyst surface. This enhanced CO_2 supply boosts CO_2RR current densities beyond mass transfer limits.